TITLE
ASP Conference Series, Vol. **VOLUME**, **PUBLICATION YEAR**
EDITORS

Distribution of dust and stars in the Galaxy

Ronald Drimmel

Osservatorio Astronomico di Torino, Pino Torinese, TO 10025, Italy

David Spergel

Princeton Observatory, Princeton, NJ

Abstract. Using far-infrared 240μm and near-infrared K band data from the COBE/DIRBE instrument, we model the Galactic stellar and dust distribution. Making the assumption that the Galaxy is transparent in the 240μm band, the dust emission is modeled using the following components: a warped exponential disk of scale length $0.26R_\odot$, a spiral arm component as mapped by HII regions, and a feature coinciding with the local (Orion) arm. The dust distribution is used to calculate absorption in the K band, and the stellar emission is likewise modeled with a warped exponential disk, with a scale length of $0.29R_\odot$, and a spiral arm component. Models of the K band emission in the Galactic plane indicate that in this waveband a two arm spiral dominates the nonaxisymmetric emission. The warp is evident in both the dust and stellar component, and is found to start within the Solar Circle.

1. Introduction and Data

The emission from our own Galaxy is naturally far greater than that from all other galaxies combined, and is received from all directions due to our location within it. Yet it is just this last fact which presents special challenges in any effort to infer the structure of our Galaxy on a large scale, particularly of the stellar component in which most of the disk mass resides. From radio observations large-scale nonaxisymmetric structure was first seen, but only with the advent of infrared observations has such structure likewise been evidenced in the stars.

Here we model the 240μm and K band emission as detected by the COBE satellite, concentrating on the Galactic plane (GP) emission for galactic radii $r > .5R_\odot$, and its nonaxisymmetric nature. This contribution can be regarded as a preview of a more detailed exposition and analysis, incorporating the J band, that will be published elsewhere. Here we will principally focus on the spiral structure in the stellar distribution inferred from the K band alone.

Galactic emission in the FIR 240μm and NIR K band was detected by the DIRBE instrument aboard the COBE satellite, from which 'Zodi-Subtracted Mission Average (ZSMA)' skymaps where produced (Kelsall et al. 1998). From these maps we take emission from galactic latitudes $|b| < 30^\circ$, excluding the Galactic Center region, and smaller regions centered on the Orion Nebula, M31,

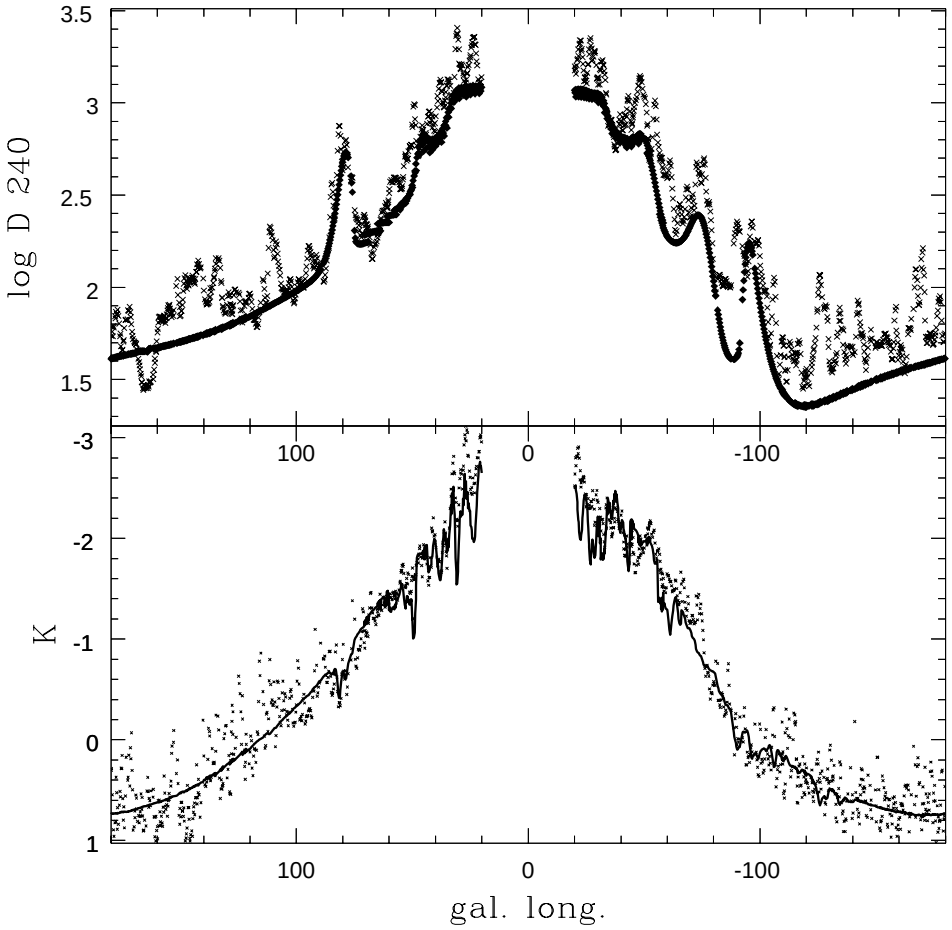

Figure 1. 240μm and K band, modeled and observed, emission profiles in the Galactic plane, on a logarithmic scale ($\log D$). Data is represented by the X's.

M33, and the Magellanic Clouds. Excluding the Galactic center obviates the need to model the Galactic bulge. In the NIR dataset point sources are also excluded, while in the FIR the data was smoothed using a second-order two-dimensional polynomial applied to a 7×7 pixel window. This smoothing procedure introduces no systematic redistribution of flux associated with the Galactic plane, and was employed only to smooth over artificial negative intensities introduced in the data set by the subtraction of Zodiacal light. The resulting data set consists of 173569 pixels at 240μm and 152371 pixels in the K band.

2. Dust distribution model

Three density components are used to model the dust distribution: an axisymmetric disk, a spiral arm component, and a local feature described as a spiral segment corresponding to the Orion arm. The axisymmetric disk component is

assumed to have an exponential radial density profile with a prescribed central hole and a sech^2 vertical profile with a linearly flaring scale height. The disk emissivity is derived by adopting a linear temperature gradient, consistent with that seen in the dust associated with HI (Sodroski et al. 1994), with the assumption that the dust emissivity is $\propto \nu^2 B_\nu(T)$, $B_\nu(T)$ being Planck's function (Draine & Lee 1984; Dwek 1995; Schlegel, Finkbeiner & Davis, 1998).

The spiral arms have a double gaussian density profile in their cross section, an assumed geometry that is adopted from a map of HII regions (Georgelin & Georgelin 1976; Taylor & Cordes 1993), and a quadratically flaring scale height. We also found it necessary to apply a reduction factor to the size (width and height) and density of the Sagittarius-Carina (Sag-Car) arm. The spiral arms are assigned a constant emissivity (single mean temperature). The local feature has a cylindrical gaussian cross section in density and two associated emissivities, one for positive galactic longitudes, the other for negative longitudes. The Sun is found in a gap of this local feature. Finally, to all the density components is added a global warp described by

$$Z_{\rm w}(r,\phi) = a_{\rm w}(r - r_{\rm w})^2 \sin(\phi - \phi_{\rm w}) \tag{1}$$

for $r > r_{\rm w}$, where the parameters $a_{\rm w}$, $r_{\rm w}$, and $\phi_{\rm w}$ are adjusted.

The FIR emission is modeled on the assumption that the Galaxy is optically thin at 240μm, leading to

$$D_{240}^{\rm mod}(l,b) = \int_{\rm los} \sum_i k_i \rho_i ds + Q_{240} = \sum_i D_i + Q_{240} \ , \tag{2}$$

where k_i and ρ_i are the emissivities and densities of the i components, and Q_{240} is an isotropic term which can be equated with the Cosmic Infrared Background (CIB). However, the decomposition of the flux density into densities and emissivities cannot be done based on the FIR emission alone; for the adjustment to the FIR data emissivity values are fixed. The size of the emitting regions are also indeterminate and the model is assigned a scale by defining length units such that $R_\odot = 1$.

The parameters of the dust model were adjusted using a χ^2 minimization routine against the DIRBE 240μm data. The resulting fit in the GP is shown in Figure 1 while emission profiles at other galactic latitudes is shown in Figure 2. (The apparent increase in the residuals with latitude are an effect of the logarythmic scale.) As can be seen in these emission profiles, while the model is unable to reproduce small scale features, the major nonaxisymmetric features are accurately placed. While the fit in the plane itself is not exceptional, it is a significant improvement over the axisymmetric models used in the past. In fact, the importance of the nonaxisymmetric features in the dust distribution is emphasized as one moves out of the GP, where these features clearly dominate the emission profiles. Here the ability of the model to reproduce the emission profiles is much more impressive. The scale length resulting from the adjustment is $0.26 R_\odot$, while the scale height is found to be 147 pc (assuming $R_\odot = 8$ kpc). We also mention that a CIB of 1.07 MJy/sr is recovered, consistent with other estimates (Hauser et al. 1998, Lagache et al. 1999).

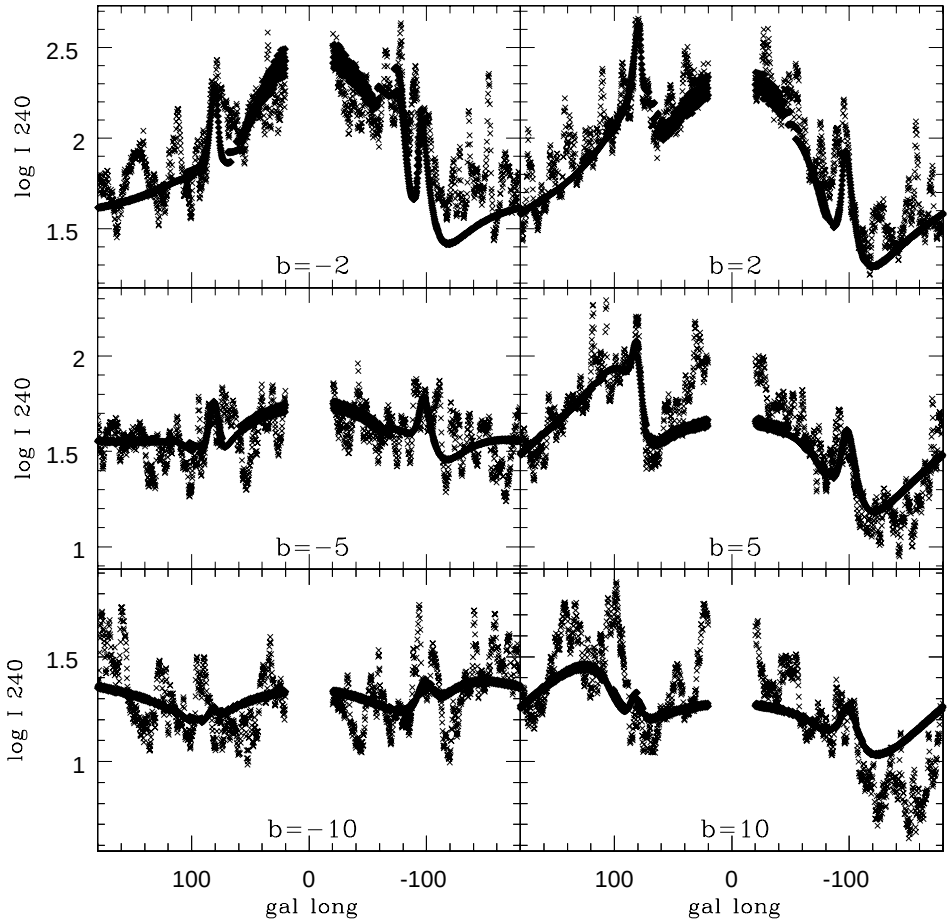

Figure 2. Observed and modeled 240μm emission profiles in 0.3 deg wide latitude bands at various galactic latitudes.

3. Stellar distribution model

In the NIR we assume negligible scattering, and that absorption is proportional to the dust column density. In this case we can write

$$D_{\rm K}^{\rm mod}(l,b) = \int_{\rm los} \eta(s) e^{-\tau(s)}\, ds + Q_{\rm K}\ , \tag{3}$$

where η is the flux density, τ the optical depth, and $Q_{\rm K}$ is again an isotropic term, though here not astrophysically justified. The stellar flux density is comprised of an axisymmetric disk component with an exponential radial profile and a sech^2 vertical profile. To this is added a spiral arm component. In the following section various spiral arm geometries are applied, but in general the arms are given a double gaussian density profile in their cross section. A warp is also

assigned to the stellar flux density, but with a different amplitude than that in the dust.

The absorption is derived from the dust model. First the dust model is rescaled, or corrected, to recover the observed FIR intensity along each line-of-sight. That is, along each line-of-sight a rescaling factor is applied to *one* of the dust density components such that $\rho_j \rightarrow f_j \rho_j$, where the rescaling factor for the jth component is specified by

$$f_j = \frac{D_{240}^{\rm obs} - \sum_{i \neq j} D_i - Q_{240}}{D_j} \ . \tag{4}$$

The component chosen is that which needs the least fractional change in density to recover the observed FIR intensity, specifically, that which minimizes $|1 - f_j|$. The resulting rescaled column density along each line-of-sight is then used to calculate the optical depth in Equation 3.

The parameters of the stellar distribution are adjusted to fit the model K band emission to the observed, and at the same time the dust densities and emissivities are decoupled. Figure 1 shows the resulting fit in the GP, and Figure 3 shows the emission profiles at other galactic latitudes. At these wavelengths nonaxisymmetric structures are far from evident, and one might even conclude that the GP profile deviates from an axisymmetric profile due to absorption effects alone (Kent, Dame & Fazio 1991). However, the model shown in Figures 1 and 3 in fact has a two arm logarithmic spiral. The next section will show fits using other (non)spiral models for comparison.

Before going on it is worth pointing out one nonaxisymmetric feature that is subtly but clearly present, namely the Galactic warp. The warp accounts for the skewness seen in the emission profiles at latitudes $|b| \geq 5^\circ$, as it starts within the Solar Circle (at $0.89 R_\odot$). The only way to reproduce such skewed profiles is to introduce a local tilt to the stellar disk with respect to the conventionally defined $b = 0$ plane, which can also be done with a large-scale tilt to the stellar disk (Hammersley et al. 1995).

4. Alternative spiral models

Two general spiral geometries are here considered. The first is a logarithmic model whose pitch angle and phase are adjusted. Both $m = 2$ and $m = 4$ arm geometries were tried. The second geometry is a sheared version of the HII arms adopted for the dust. If the arms are assumed to have a fixed pattern in the presence of a flat rotation curve, then the drift in azimuth is

$$\phi_\tau = V_o \tau \left(\frac{1}{r} - \frac{1}{R_{\rm C}} \right) , \tag{5}$$

where V_o is the circular rotation speed, τ the mean age of the population, and $R_{\rm C}$ the corotation radius. In this formulation the geometry is found by adjusting parameters equivalent to $V_o \tau$ and $R_{\rm C}$. A fourth model considered, for purposes of comparison, is a purely axisymmetric model.

All these models give fits which differ only close to the plane of the Galaxy, that is at $|b| < 3^\circ$. The resulting disk scale lengths are found to be about

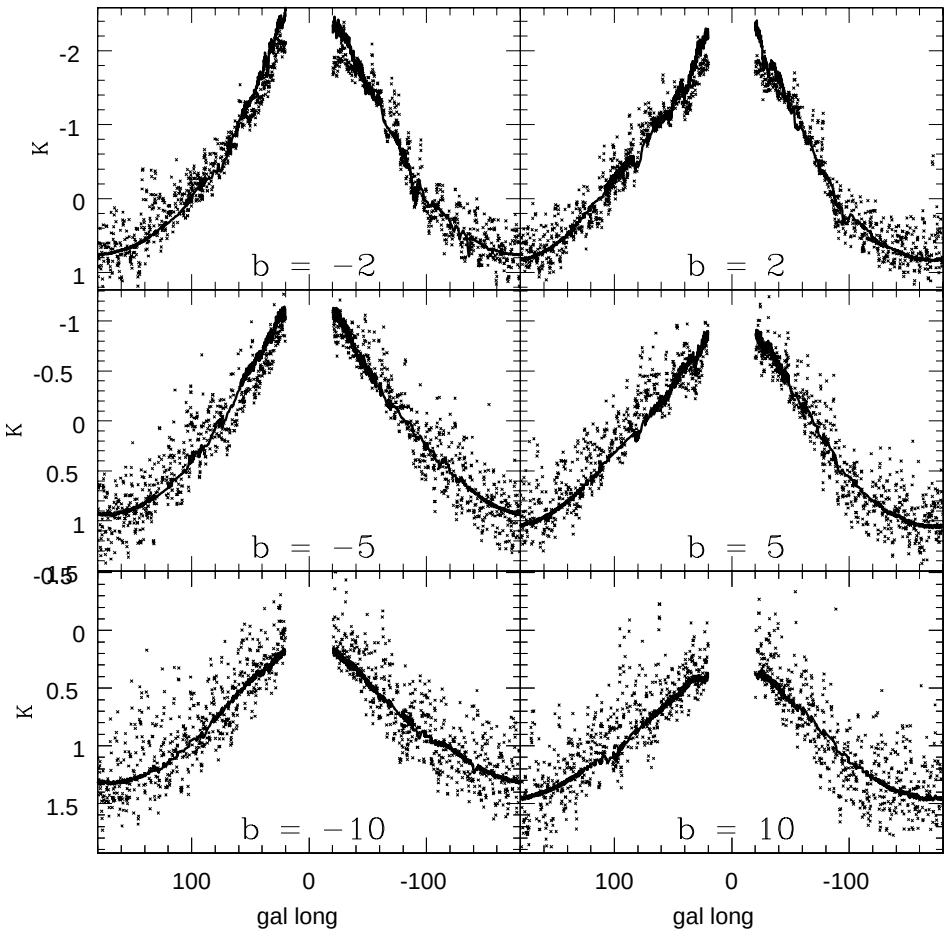

Figure 3. K band data and model profiles (solid lines) in 0.3° wide latitude bands at various galactic latitudes.

$0.29R_\odot$, except for the $m = 4$ model which gives a larger scale length of $0.37R_\odot$, while the scale heights range from 270 to 307 pc and $Z_\odot$ from 12 to 15 pc in the models (again assuming $R_\odot = 8$ kpc). Figure 4 shows the GP profiles for the four models just described. As can be immediately seen, the sheared arm model and the $m = 2$ logarithmic model give correspondingly good fits to the data, while the $m = 4$ and axisymmetric models fail to reproduce the observed profile specifically in the directions of the tangents to the Scutum arm ($l \simeq -55°$ and 30°). No evidence of the Sag-Car arm is seen at positive Galactic latitudes, as shown by the axisymmetric model. The pitch angle for the $m = 2$ log spiral is found to be 15.6°, while that for the $m = 4$ model is 12.4°. For the sheared spiral model a corotation radius of $R_C = 0.83R_\odot$ is arrived at, and a mean age of $\tau = 15$ Myr is found if one adopts the values 200 km/s and 8 kpc for the circular speed and $R_\odot$ respectively.

5. Conclusions

For the K band emission two spiral models were found that reproduce the GP emission profiles, a $m = 2$ logarithmic spiral model and a sheared version of the arms seen in the dust. This latter model is a 4 arm model, however a reduction factor is applied to the Sag-Car arm that renders it significantly smaller than the other arms (a factor of 0.53 in two dimensions and in density). We thus conclude that in the NIR a two arm spiral dominates the nonaxisymmetric emission. This conclusion supports the earlier simple analysis of Drimmel (2000) based on the position of identified tangent features. However, the nature of the arms are not clear; the open $m = 2$ logarithmic arms suggest an old population, as argued in Drimmel (2000), while the successful sheared spiral model is consistent with the nonaxisymmetric emission arising from young K supergiants. Favoring this latter interpretation is the small scale height of the arms, which are not seen at $|b| > 3^\circ$ from the GP. It is hoped that our future study including the J band will resolve this issue.

Acknowledgments. The COBE datasets were developed by the NASA Goddard Space Flight Center under the guidance of the COBE Science Working Group and were provided by the NSSDC.

References

Draine, B. T., & Lee, H. M. 1984, ApJ, 285, 89

Drimmel R. 2000, A&A, 358, L13

Dwek, E., Arendt, R. G., Hauser, M. G., Kelsall, T., Lisse, C. M., Moseley, S. H., Silverberg, R. F., Sodroski, T. J., & Weiland, J. L. 1995, ApJ, 445, 716

Georgelin, Y. M., & Georgelin, Y. P. 1976, A&A, 49, 57

Hammersley, P. L., Garzon, F., Mahoney, T., & Calbet, X. 1995, MNRAS, 273, 206

Hauser, M. G., Arendt, R. G., Kelsall, T., Dwek, E., Odegard, N., Weiland, J. L., Freudenreich, H. T., Reach, W. T., Silverberg, R. F., Moseley, S. H., Pei, Y. C., Lubin, P., Mather, J. C., Shafer, R. A., Smoot, G. F., Weiss, R., Wilkinson, D. T., & Wright, E. 1998, ApJ, 508, 25

Kelsall, T., Weiland, J. L., Franz, B. A., Reach, W. T., Arendt, R. G., Dwek, E., Freudenreich, H. T., Hauser, M. G., Moseley, S. H., Odegard, N. P., Silverberg, R. F., & Wright, E. L. 1998, ApJ, 508, 44

Kent, S. M., Dame, T. M., & Fazio, G. 1991, ApJ, 378, 131

Lagache, G., Abergel, A., Boulanger, F., Désert, F. X., & Puget, J. L. 1999, A&A, 344, 322

Schlegel, D. J., Finkbeiner, D. P., & Davis, M. 1998, ApJ, 500, 525

Sodroski, T. J., Bennett, C., Boggess, N., Dwek, E., Franz, B. A., Hauser, M. G., Kelsall, T., Moseley, S. H., Odegard, N.,Silverberg, R. F., & Weiland, J. L. 1994, ApJ, 428, 638

Taylor, J. H., & Cordes, J. M. 1993, ApJ, 411, 674

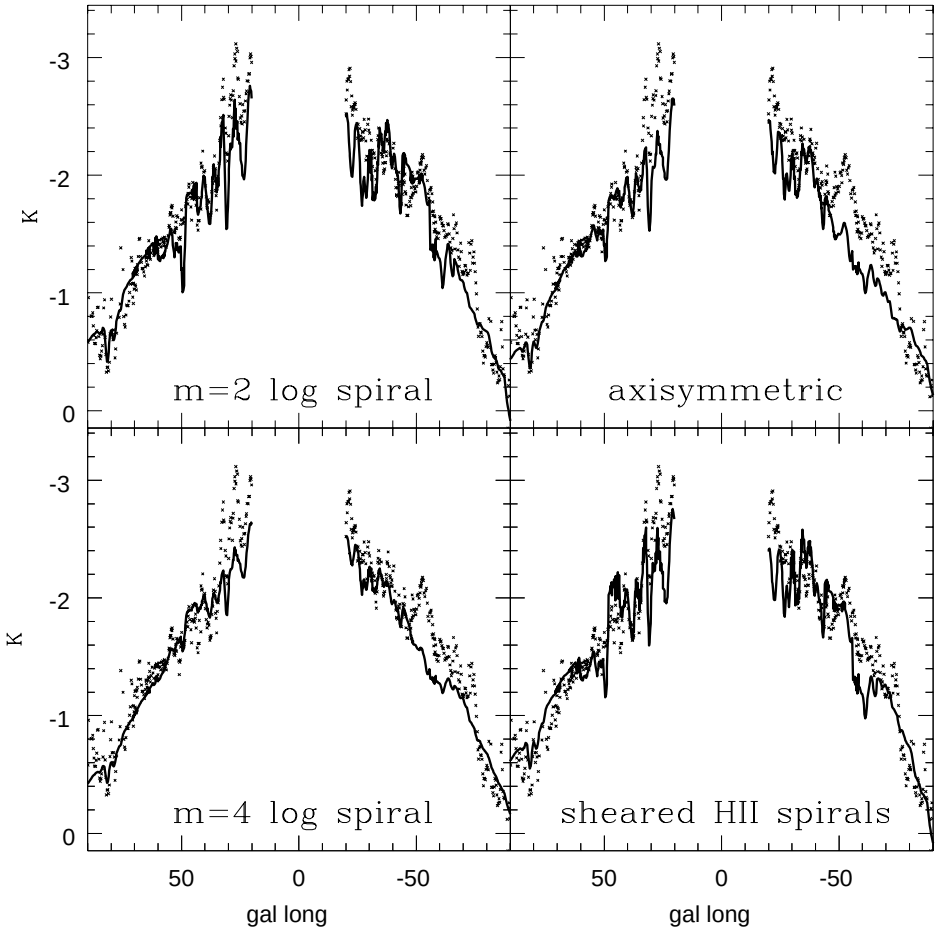

Figure 4. K band emission profiles within 0.17° of the GP for four spiral arm models against the observed emission profile, for galactic longitudes $|l| < 90°$. Models differ most in the direction of the Scutum arm tangent at $\approx -55°$.